AIP | Review of Scientific Instruments

Experimental energy resolution of a paracentric hemispherical deflector analyzer for different entry positions and bias

M. Dogan, M. Ulu, G. G. Gennarakis, and T. J. M. Zouros

Citation: Rev. Sci. Instrum. **84**, 043105 (2013); doi: 10.1063/1.4798592
View online: http://dx.doi.org/10.1063/1.4798592
View Table of Contents: http://rsi.aip.org/resource/1/RSINAK/v84/i4
Published by the American Institute of Physics.

Experimental energy resolution of a paracentric hemispherical deflector analyzer for different entry positions and bias

M. Dogan,[1,a)] M. Ulu,[1] G. G. Gennarakis,[2] and T. J. M. Zouros[2]
[1]*eCOL Laboratory, Department of Physics, Science and Arts Faculty, Afyon Kocatepe University, 03200 Afyonkarahisar, Turkey*
[2]*Atomic Collisions and Electron Spectroscopy Laboratory, Department of Physics, University of Crete, P.O. Box 2208, 71003 Heraklion, Crete, Greece*

(Received 6 March 2013; accepted 14 March 2013; published online 10 April 2013)

A specially designed hemispherical deflector analyzer (HDA) with 5-element input lens having a movable entry position R_0 suitable for electron energy analysis in atomic collisions was constructed and tested. The energy resolution of the HDA was experimentally determined for three different entry positions $R_0 = 84$, 100, 112 mm as a function of the nominal entry potential $V(R_0)$ under pre-retardation conditions. The resolution for the (conventional) entry at the mean radius $R_0 = 100$ mm was found to be a factor of 1.6-2 times *worse* than the resolution for the two (paracentric) positions $R_0 = 84$ and 112 mm at particular values of $V(R_0)$. These results provide the first *experimental* verification and a proof of principle of the utility of such a paracentric HDA, while demonstrating its advantages over the conventional HDA: greater dispersion with reduced angular aberrations resulting in better energy resolution without the use of any additional fringing field correction electrodes. Supporting simulations of the entire lens plus HDA spectrometer are also provided and mostly found to be within 20%–30% of experimental values. The paracentric HDA is expected to provide a lower cost and/or more compact alternative to the conventional HDA particularly useful in modern applications utilizing a position sensitive detector. © *2013 American Institute of Physics*. [http://dx.doi.org/10.1063/1.4798592]

I. INTRODUCTION

The hemispherical deflector analyzer (HDA) is one of the most widely used electrostatic energy selectors in low energy atomic collision physics (for a recent review see Ref. 1 and the references therein). However, the first-order focusing characteristics of a HDA are impaired due to the fringing fields created at the electrode entry boundaries. In the conventional HDA, fringing fields generally produce an image with larger angular aberrations at the dispersion plane from that predicted for the ideal (no fringing fields) HDA leading to a substantial deterioration in its energy resolution.[1] Partial recovery of the high resolution attributes of the ideal HDA can be attained by incorporating additional electrodes in various fringing field correction schemes.[2] Over the last decade, it has been shown in simulation[2–5] that this drawback can also be readily overcome without using any type of additional fringing field corrector electrodes in an arrangement that has come to be known as the "biased paracentric" HDA.[5] This HDA utilizes a biased optical axis (i.e., the central ray trajectory is not at 0 potential as in a conventional HDA) and an optimized entry position R_0 *offset* from the center position (at the mean radius $\bar{R} = (R_1 + R_2)/2$) used in conventional HDAs.[5] Previous simulations have shown[2–5] that the biased paracentric HDA can in principle restore near ideal field conditions. To date, however, these expectations have not been tested experimentally since they require a direct comparison of conventional and paracentric entries in the *same* analyzer necessitating a HDA with a *variable* entry radius R_0. Since HDAs are typically also equipped with an input lens this would require, in addition, special hardware allowing for the precise repositioning of the entire electron source, lens and entry aperture assembly at the various entry radii to be tested, clearly requiring a special arrangement. In this paper we report on first experimental results using such a variable entry HDA, specifically designed for testing the biased paracentric HDA concept experimentally and the energy resolution improvements claimed by simulation.

The design considerations outlined in our previous simulation work[5] were realized experimentally here and the new biased paracentric HDA configuration for atomic collisions was constructed and tested. The present analyzer uses a wide-gap inter-electrode distance $\Delta R \equiv R_2 - R_1 = 50$ mm and a mean radius $\bar{R} = 100$ mm. It incorporates a standard input lens, which in this case is mounted on a rail to allow for the repositioning of the entry at any value R_0 between the inner hemisphere at radius $R_1 = 75$ mm and the outer hemisphere at $R_2 = 125$ mm. The apparatus is shown in Fig. 1. Here, we report on energy resolution measurements for two paracentric entry positions $R_0 = 84$ mm and $R_0 = 112$ mm, on either side of the mean radius, respectively, in comparison to the conventional (central) entry at $R_0 = \bar{R} = 100$ mm. These specific R_0 entry positions were predicted[5] from our previous simulation work[2,4] to correspond to positions of optimal energy resolution for the right entry bias.

We note that our reported experimental measurements are performed on a combined ESCA-type spectrometer (comprised of a HDA with input lens) under pre-retardation conditions, typical in high resolution electron spectroscopy applications. This necessitated the use of new additional simulations

a)Author to whom correspondence should be addressed. Electronic mail: mdogan@aku.edu.tr

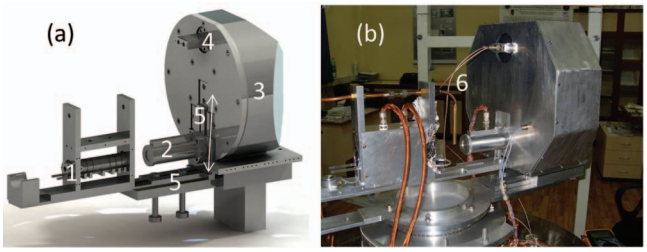

FIG. 1. (a) 3D drawing of the complete analyzer system, showing its five main parts: (1) electron gun, (2) input lens, (3) HDA, (4) detector CEM assembly, and (5) movable supporting rail. The electron gun and input lens are seen to be assembled on the same movable supporting rail. (b) Photograph of the actual setup also showing the vertical gas nozzle jet target (6). Here, the electron gun is seen to lie across the analyzer while in the measurements it was used at 90°. The supporting rail can be moved up or down along the direction of the double arrows, effectively changing the entry position of the analyzer R_0.

under pre-retardation conditions, which are also presented for comparison.

II. ELECTRON OPTICAL PROPERTIES

The energy dispersing properties and focusing action of the biased paracentric HDA have been discussed in a number of articles.[1–5,7] We therefore present here only a short summary of important relevant characteristics.

The general potential $V(r)$ in an *ideal* HDA can be obtained[1] from the analysis of the general trajectory equations applied to the *central ray*. This is used as the reference trajectory entering the HDA with *pass energy* E_0 and input angle $\alpha = 0°$ at the entry radius R_0 and exits after deflection by 180° through the analyzer at the radius R_π here set to be equal to the mean radius, i.e., $R_\pi = \bar{R}$. Thus, the $V(r)$ potential (referenced to absolute ground) is given by[1]

$$qV(r) = E_0 \left\{ F - \gamma \left(\frac{R_0}{R_\pi} \right) \left[\frac{(R_0 + R_\pi)}{r} - 1 \right] \right\}. \quad (1)$$

The voltages on the hemispherical electrodes $V_1 = V(R_1)$ and $V_2 = V(R_2)$, as well as at the entry $V_0 = V(R_0)$, can then be directly obtained from Eq. (1) for r = R_1, R_2 and R_0, respectively. F is the pre-retardation ratio E_{s0}/E_0 where E_{s0} is the electron source energy ($F = 1$ when no pre-retardation is used). The parameter γ, known as the entry *biasing parameter*,[1,7] is related to the entry bias V_0 through Eq. (1) for $r = R_0$ giving $qV_0 = (F\text{-}\gamma)E_0$. Here, γ is used as an *independent* variable needed in the specification of both hemisphere voltages V_i and entry bias V_0. γ can be shown to be equivalent to the relative index of refraction across the lens/HDA interface.[7]

A conventional HDA typically uses symmetrical entry and exit conditions $R_0 = R_\pi = \bar{R}$ (and therefore is also referred to as a centric HDA). When no pre-retardation is used ($F = 1$), it also has zero bias, i.e., $V_0 = 0$ or $\gamma = 1$. On the other hand, a biased paracentric HDA uses asymmetric entry and exit conditions, and thus typically has $R_0 \neq \bar{R}$ and non-zero bias $V(R_0) \neq 0$ or equivalently $\gamma \neq 1$. Thus, a biased paracentric HDA is seen to represent a more general class of HDAs in which the conventional HDA is just a special case, where the central ray is in general part of an ellipse, while in the conventional HDA it is part of a circle.[1]

An electron entering a HDA (tuned to pass a central ray of energy E_0), in the vicinity of the entry at $r_0 = R_0 \pm \Delta r_0/2$ with a pass energy $E \pm \Delta E/2$ and small input half-angle α, will exit the HDA (after 180° deflection) at the radius $r_\pi = R_\pi \pm \Delta r_\pi/2$. Under these conditions, the exit beam width along the energy dispersion direction, Δr_π, is given to 2nd order in α by[10]

$$\Delta r_\pi = |M|\, \Delta r_0 + D_\gamma \frac{\Delta E}{E} + P_1 \alpha + P_2 \alpha^2. \quad (2)$$

Here, M is the linear magnification, D_γ is the γ-dependent dispersion length $D_\gamma \equiv E\, \partial r_\pi / \partial E$, while P_1 and P_2, are the first- and second-order angular aberration coefficients, respectively. This formula has also been used to parameterize the *real* fringing field HDA by determining the coefficients M, D_γ, P_1, and P_2, taking into account the distribution of the electrons over the entry radius r and half-angle α. These were obtained[2] as least square fitting parameters for various HDA fringing field corrections schemes. In the case of the *ideal* HDA we have $M = -1$, $P_1 = 0$, and $P_2 = -D_\gamma$, where D_γ is given by[7]

$$D_\gamma = \left(\frac{R_\pi + R_0}{\gamma} \right) \frac{R_\pi}{R_0}. \quad (3)$$

$P_1 = 0$ means that the ideal HDA has first-order focusing.

For a *monoenergetic* ($\Delta E = 0$) beam of electrons going through a HDA with voltages V_i set to pass the central ray of energy E_0, it can be readily shown[7–10] from Eq. (2) that the HDA *base* energy resolution R_{B0} is related to the *maximal* beam width $\Delta r_{\pi\,\max}$ by

$$R_{B0} \equiv \frac{\Delta E_B}{E_0} = \frac{\Delta r_{\pi\,\max} + w_2}{D_\gamma}, \quad (4)$$

where w_2 is the HDA exit slit width along the dispersion direction. In the case where a PSD is used instead of an exit slit, w_2 is near zero. Both $\Delta r_{\pi\,\max}$ and D_γ can be readily determined from electron trajectory simulations (without the need to separately obtain the M, P_1, and P_2 coefficients) thus making the right side of Eq. (4) very convenient for the direct evaluation of the HDA resolution in simulations as done here. The left side of Eq. (4) is typically used for the experimental determination of the spectrometer base resolution, usually taking $\Delta E_B \approx 2\Delta E_{FWHM}$, the energy resolution at the full width half maximum (FWHM), as also done here.

For the ideal HDA, assuming uniform entry illumination, Δr_0 in Eq. (2) can be replaced by the entry slit width w_1 and the *base* energy resolution is then given by the well-known formula

$$R_{B0ideal} = \frac{\Delta E_B}{E_0} = \frac{w_1 + w_2}{D_\gamma} + \alpha^2_{\max} \quad (Ideal\ \text{HDA}), \quad (5)$$

where $\alpha_{\max}$ is the maximum input half-angle in the plane of the dispersion. For the ideal *centric* HDA (i.e., the conventional HDA with $R_0 = R_\pi$ and $\gamma = 1$), Eq. (3) gives $D_\gamma = 2R_0$ and thus Eq. (5) leads to the well-known ideal conventional HDA base energy resolution formula.

In most high resolution applications *pre-retardation* is typically used to improve the energy resolution of the HDA

by decelerating the electron beam prior to HDA (lens) entry. This is accomplished by negatively biasing the last input lens element at the potential $V_{5a} = -(E_{s0}\text{-}E_0)$ (the same potential used on the base plate of the HDA). In this case the *overall* base resolution of the HDA is improved by the pre-retardation factor F and simply given by

$$R_{Bs0} = \frac{\Delta E_{\mathrm{B}}}{E_{s0}} = \frac{1}{F}\left(\frac{\Delta E_{\mathrm{B}}}{E_0}\right) \quad (Overall \text{ base resolution}). \tag{6}$$

Here E_{s0} is the original central trajectory electron source energy prior to retardation.

In the case of pre-retardation the value of $\alpha_{\max}$, the size of the lens image Δr_0 and F are all linked via the Helmholtz-Lagrange law and an optimal solution exists given by[11]

$$R_{Bs0\,optimal} = \frac{\Delta E_{\mathrm{B}}}{E_{s0}} = \frac{3}{2^{2/3}}\left(\frac{d_p d_s}{2lFD_\gamma}\right)^{2/3} + \frac{w_2}{FD_\gamma}$$
$$\text{(Optimal overall ideal base resolution)}, \tag{7}$$

where d_{p} is the diameter of the pupil (lens entry aperture), d_{s} is the source diameter (height of object), and l is the distance between source and entry pupil. The optimal resolution $R_{Bs0\,optimal}$ should be best seen as the absolute resolution limit of an ideal HDA using an input lens for focusing and pre-retardation and in practice is rarely, if ever, attained. In addition, the actual resolution will also be modified[12] by the distance h between HDA exit plane and the detection or exit slit plane. When a PSD is used, h is typically 12–15 mm and can therefore additionally contribute to the resolution. In our present slit setup, $h \approx 5$ mm and its effect was found to be small and therefore has not been included. In Table I, we list the values of the important parameters.

TABLE I. List of most important geometric parameters used in both experimental setup and theoretical modeling (SIMION simulations and ideal field theoretical calculations).

Parameter	Values	Explanation
R_0	84, 100, 112 mm	HDA entry radius
R_1	75 mm	HDA inner radius
R_2	125 mm	HDA outer radius
w_1	2 mm	HDA diameter of entry aperture
w_2	2 mm	HDA diameter of exit aperture
h	5 mm	Gap between HDA plane and exit slit plane
s	140 mm	Length of 5-element cylindrical lens
g	2.5 mm	Lens inter-electrode gap
d	20 mm	Lens internal diameter
d_p	2 mm	Diameter of pupil (lens entry aperture)
l	50 mm	Distance between target and lens
d_s	2 mm	Source diameter
E_{s0}	200 eV	Nominal electron gun energy
E_0	50 eV	Nominal electron HDA pass energy
F	4	Pre-retardation ratio – E_{s0}/E_0
$\alpha_{\max}$	6.5°	Maximal HDA input half-angle ($F = 4$)

III. EXPERIMENTAL SETUP

The spectrometer setup[13] used to test our analyzer is based on the crossed-beams principle and basically consists of a high intensity electron gun, a gas beam target, and the HDA. A near-monoenergetic beam of electrons produced by an e-gun was focused onto the target beam and collected in a Faraday cup, while the scattered electrons were detected as a function of their kinetic energy and the angle through which they were scattered.

A 3D drawing and photograph of the complete analyzer system is shown in Fig. 1(a) and Fig. 1(b), respectively. A mounting plate supported the input lens, hemispheres, and detector. The input lens was mounted on a rail, electrically isolated from the shielding electrode. A screw was used to position the lens system, which could be moved up and down along the dispersion direction thus allowing the entry distance R_0 to be effectively varied. The electron gun was also mounted on the same rail and therefore both e-gun and lens remained aligned on the lens axis as they were both moved up or down together.

A circular (2 mm diameter) lens entrance aperture was used and positioned 50 mm from the scattering center. The analyzer entrance and exit apertures were also circular with a 2 mm diameter. The electron gun could be rotated relative to the analyzer about the axis of the gas jet target. All analyzer parts were made from dural. All surfaces exposed to electrons were covered with soot and all aperture plates were made from molybdenum. The vacuum chamber was pumped by a 500 l/s turbomolecular pump. The background pressure in the vacuum chamber was better than 8×10^{-8} mbar. The chamber was magnetically shielded by both μ-metal, which lined the inner wall, and an external Helmholtz coil system. The magnetic fields across the electron beam directions were consequently reduced to a few mG.

A 140 mm long five-element cylindrical electrostatic input lens[13–15] transported the scattered electrons to the analyzer. The electrons were then energy analyzed by the hemispherical deflector and detected by a single channel electron multiplier (CEM). The electronic circuits (voltage supply and signal processing) needed for the operation of the analyzer is shown in Fig. 2. All the potentials for the input lens and the deflector electrodes, namely $V_{1a\text{–}5a}$, V_1, and V_2, could be independently tuned by a set of potentiometers with low ripple HV power supplies. The signal from the CEM was amplified by a fast amplifier (Philips Scientific 777) and discriminated by a constant fraction discriminator (Philips Scientific 705). By scanning the deceleration voltage (V_{5a}) and HDA voltages V_{i}, the scattered electron profile was transmitted through the analyzer while the pass energy $E_0 = E_{s0} - e|V_{5a}|$ remained fixed. The voltage ramp applied to V_{5a} was generated by an Ortec MCS-PCI card and the transmitted beam profile stored in the computer and displayed. The ramp voltage sequence was repeated until a pre-determined statistical accuracy of the signal was obtained. The electron gun was placed at two different positions. In the first position, used to study transmission as a function of γ, the analyzer was located directly across from the electron gun (0^0) with the CEM used as a Faraday cup. In these tests the value of γ was varied while the electron current

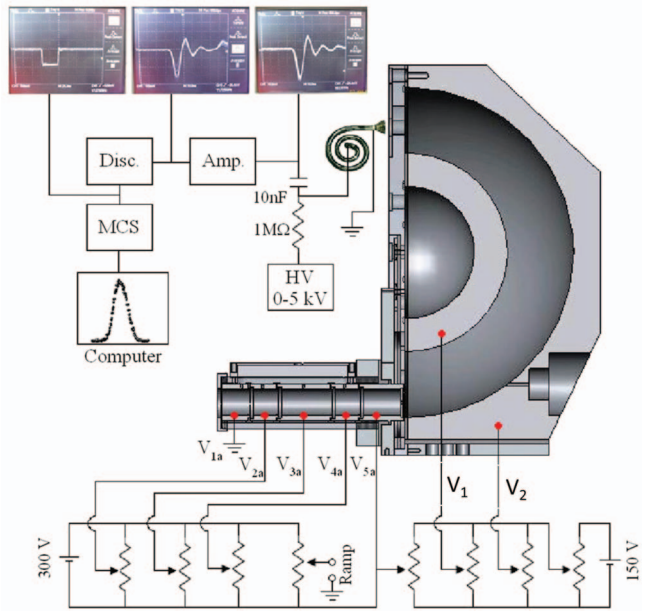

FIG. 2. Analyzer circuit used to operate the analyzer. V_{5a} is used to retard the electrons down to the pass energy E_0 which was kept fixed during spectrum scans.

passing through the analyzer exit slit was recorded by the current collected in the CEM and measured with a Keithley picoammeter. In the second position, used to determine the energy resolution of the analyzer as a function of γ, the elastic scattering peak was measured for electron-Helium collisions. To measure the elastic energy distribution of the scattered electrons both the electron gun position as well as the angle of the analyzer could be varied. In both positions, the analyzer voltages V_1 and V_2 were set according to Eq. (1) for each of the values of γ and R_0 used. In Sec. IV our γ-dependent results are shown for those electrons that were elastically scattered through 90° before entering the spectrometer. At this scattering angle, spectroscopy results were more detailed and accurate and compared well with the more coarse current measurements of the first position.

IV. RESULTS

A. Experiment

The performance of the analyzer was tested by energy analyzing the elastic electron scattering peak for different γ values of the entry bias at the three entry positions, $R_0 = 100$ mm, 84 mm, and 112 mm, respectively. From the recorded electron line shape the effective resolution of the analyzer was directly determined. In all measurements described here the energy of the electrons emitted from the electron gun was set to $E_{s0} = 200$ eV. Measurements were then carried out to obtain the peak structure of electrons for pass energies $E_0 = 30, 40, 50, 60$ eV. In Fig. 3 are shown typical line shapes obtained for the pass energy of $E_0 = 50$ eV at the fixed scattering angle of 90° with respect to the incident beam, demonstrating the near Gaussian shape of the experimental points. The width of the peaks was determined by the temperature of the filament of the electron gun and the analyzer parameters. A base energy width of $\Delta E_{s0} = 0.6$ eV was associated with the gun as determined experimentally. The base energy resolution of the analyzer $\Delta E_B = \Delta E_{anal}$ was then extracted after deconvolution of the gun resolution, using the relation $\Delta E_{anal} = \sqrt{\Delta E_{obs}^2 - \Delta E_{s0}^2}$, where ΔE_{obs} is the base width of the observed line shape. The determined overall resolutions for a pass energy of $E_0 = 50$ eV for the three values of R_0 are shown in Fig. 4 as a function of γ.

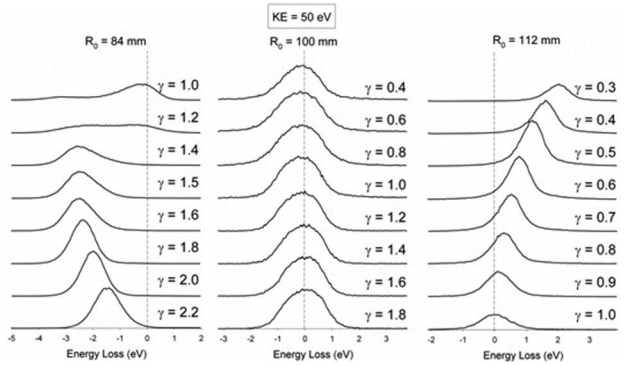

FIG. 3. Electron kinetic energy spectra showing the elastic scattering peak from 200 eV electrons incident on a Helium target for $R_0 = 84$ mm (left), $R_0 = 100$ mm (middle), and $R_0 = 112$ mm (right). The spectrometer was set to pass electrons with a kinetic energy of $E_0 = 50$ eV corresponding to 0 energy loss. The y-axis represents normalized counts.

B. SIMION simulations

SIMION simulations are based on the finite difference approach whose accuracy relating to HDAs has been investigated in a previous publication[16] based on the 2005 SIMION 7.0 version. Here, we use the latest 2012 SIMION 8.1 version[6] that has been substantially improved in speed, accuracy, and programming capabilities through the use of many new features such as "surface enhancement" to improve the modeling of curved electrodes, menu driven definitions of initial electron conditions, as well as taking advantage of multi-core, 64-bit PC technology and larger RAM availability.

These technological and software improvements have allowed us to readily simulate the combined HDA plus 5-element input lens in a *single* large 3D potential array (known as an instance in SIMION) using a fairly small fixed density grid size of 0.5 mm per grid unit for an apparatus covering a near cubic volume of more than 300 mm extent on each side. The strong fringing fields between the HDA support plate and the hemispherical electrodes necessitated such a one-instance approach since the image of the lens lies in the fringing field volume. Reflection symmetry in the plane of the dispersion ($Y = 0$ plane) was used to cut down on RAM. The details of the full 3D trajectory simulations will be described in a forthcoming publication.[19] Here we only give a brief report about our approach as it relates to the evaluation of the energy resolution requiring only a 2D trajectory approach in the plane of the dispersion.

Two different simulation approaches were used in which the same 2D monoenergetic angular electron distribution (saved as a SIMION.ion file) was used for consistency. This

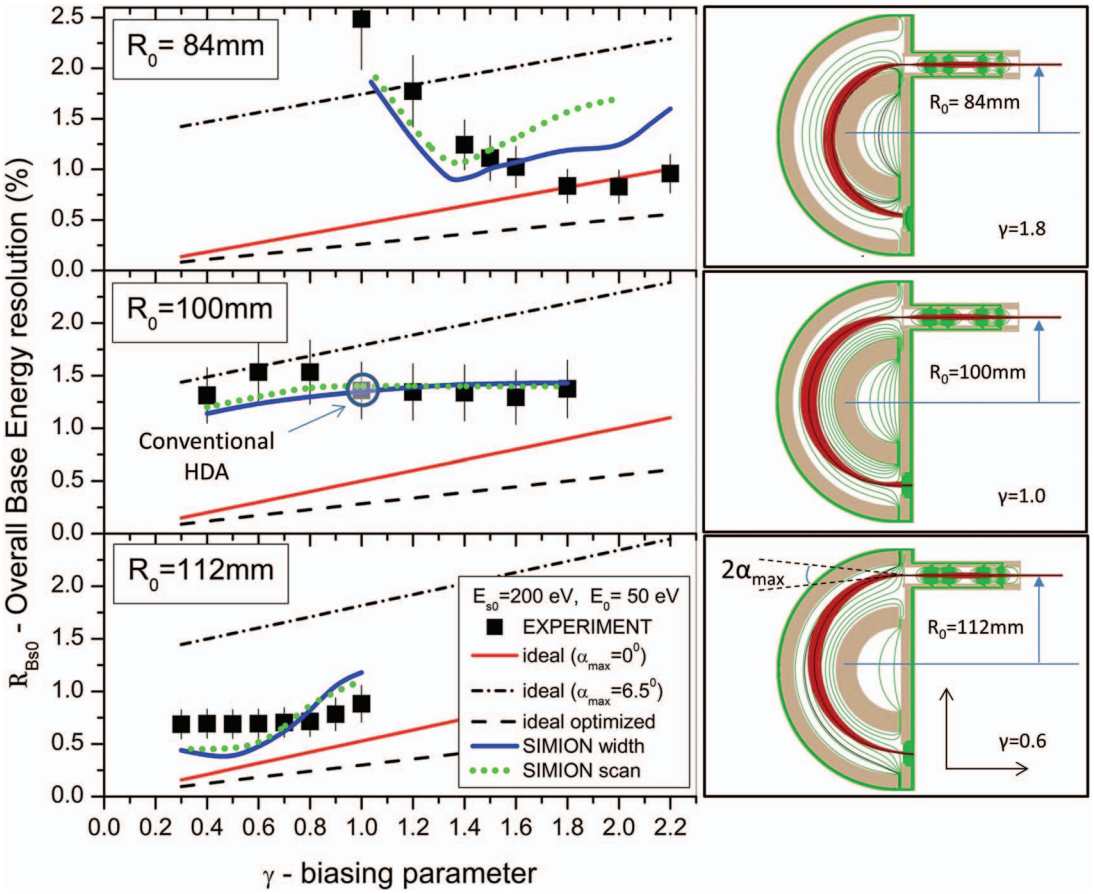

FIG. 4. (Left) HDA *overall base* energy resolution $R_{Bs0} = \Delta E_B/E_{s0}$ plotted as a function of the biasing parameter γ for a source energy $E_{s0} = 200$ eV and pass energy $E_0 = 50$ eV. Data points: experimental results by spectrum scan for fixed pass energy. Error bars: estimated at $\pm 20\%$ of R_{Bs0} to account for possible "mechanical imperfections."[18] Straight lines: theoretical calculations for an *ideal* HDA: (full) based on Eq. (5) and $\alpha_{max} = 6.5^\circ$ (black dashed-dotted) and 0° (red). (Dashed lines) Optimal resolution based on Eq. (7). SIMION simulations: (blue line) exit beam width formula based on Eqs. (4) and (6). (Dotted green line) Spectrum scan for fixed pass energy as in actual measurements. The parameters listed in Table I were used in the formulas and simulations. The conventional HDA entry is marked by a circle at $R_0 = 100$ mm and $\gamma = 1.0$ for clear reference. (Right) Schematic of SIMION simulations in the $Y = 0$ dispersion plane of the spectrometer. Electron trajectories are shown in red and equipotentials in green for specified values of γ.

distribution represented 10 000 electrons of initial kinetic energy $E_{s0} = 200$ eV ejected from a source point S with coordinates (x_s, $y_s = 0$, $z_s = l = +50$ mm) and passing through a pupil point P with coordinates (x_p, $y_p = 0$, $z_p = -1$ mm). The values of both x_s and x_p positions were independently and randomly generated (easily done by the new extensive particle menu features of SIMION 8.1) to lie within the corresponding source and pupil limits: $R_0 - d_s/2 \le x_s \le R_0 + d_s/2$ and $R_0 - d_p/2 \le x_p \le R_0 + d_p/2$, thus defining both the initial position and direction of each electron trajectory flown. In our geometry the lens entry aperture (pupil) was set at $z = 0$ and had a thickness of 1 mm. All electrons were flown in the dispersion plane ($Y = 0$), which was also the reflection symmetry plane of the whole apparatus with the cylindrical lens axis aligned along the negative Z-axis. For each of the three values of R_0 the lens voltages were set and fixed to the optimally chosen experimental voltages based on past experience with the 5-element lens.[15] HDA voltages were set according to Eq. (1) and therefore depended on both R_0 and γ.

The first simulation approach, termed the "beam width" method, was based on evaluating the right side of Eq. (4) by determining the maximal beam width $\Delta r_{\pi max}$ and dispersion D_γ. $\Delta r_{\pi max}$ measured the maximum beam width along the dispersion direction (x-axis) on the plane of the exit aperture. D_γ was evaluated for each γ by "flying" a set of different energy E_i trajectories with $\alpha = 0$ and recording their exit positions $r_\pi(E_i)$. A least square linear fit of the form $r_\pi(E_i) = a + b\,E_i$, where a and b are the fitting parameters, then led to the value of $D_\gamma = E_0$ b. Substituting the obtained D_γ value into Eq. (4) with $w_2 = 2$ mm and using Eq. (6) for F = 4 gave the overall base energy resolution shown in Fig. 4 as the blue line.

The second approach termed the "voltage scan" method was almost identical to the way the experimental spectrum (line profile) in Fig. 3 was obtained by stepping the voltages of the HDA and recording the number of electron trajectories that go through the exit aperture for each step. During the scanning of the voltages all lens potentials were kept fixed except for V_{5a} (also the HDA plate potential), which was stepped so as to keep the pass energy fixed at 50 eV. The voltages were stepped in 0.1 or 0.2 eV steps so as to cover the entire electron peak, which typically extended not more than 2 eV on either side of the central energy of 200 eV. At each step the previously mentioned electron distribution was "flown."

The base energy ΔE_B of the line profile could be directly determined from the final energy spectrum and was used in

Eq. (6) to compute the overall base resolution. These results are shown in Fig. 4 as the dotted green line. With the exception of the cases of $R_0 = 84$ mm with $\gamma > 1.5$ good overall consistency was found between the two approaches which usually differed by less than ~15% for most points evaluated. The exceptional cases of $R_0 = 84$ mm differed by more than 30% for reasons as yet unknown (see below).

C. Theory—ideal field HDA

Even though the ideal HDA resolution formulas are known to be off, mostly due to the entrance fringing field effects, they are still used as an ultimate guideline and/or limit due to their simplicity. Furthermore, most of the high priced HDAs on the market today do utilize some type of fringing field correction scheme[2] which bring the real HDA resolution specs closer to those of the ideal field. In this spirit, we have listed in Fig. 4 three ideal field calculations for comparison.

The three lines correspond to the well-known resolution formula Eq. (5) with the dispersion calculated from Eq. (3). The first term of Eq. (5) is known as the slit term and the second as the aberration term. Two cases are shown for $\alpha_{\max} = 0^\circ$ and $\alpha_{\max} = 6.5^\circ$. The first corresponds to the trajectory of a central ray, while the second to a ray entering at an angle of 6.5° with respect to the perpendicular to the HDA entry plane. The value of 6.5° was found from our simulations to be indicative for most cases. Typically, however, one strives to keep $\alpha_{\max}$ as small as possible as it leads to asymmetric line shapes with a low energy tail. When pre-retardation is used to improve the overall resolution, larger α values become inevitable since upon deceleration the electron beam tends to open up, an effect the lens focusing tries to compensate for. For optimal resolution, a compromise is usually sought that can be arrived at via the Helmholtz-Lagrange law[11] leading to the result of Eq. (7) shown in Fig. 4 as the dashed line. For high values of F, Eq. (7) approaches the Kuyatt-Simpson criterion[11,17] in which the aberration term is restricted to half the value of the slit term to keep the effect of tailing small.

In Table II we summarize our results for the best experimental resolution values.

V. DISCUSSION

The results presented in Figs. 3 and 4 represent a unique set of resolution data for the three different entry positions of the same HDA allowing a direct intercomparison. The conventional HDA energy resolution (circle in blue at $R_0 = 100$ mm and $\gamma = 1$) is clearly seen to be worse (larger) than both biased paracentric cases for $R_0 = 84$ mm and $R_0 = 112$ mm depending on γ. Best experimental paracentric resolutions are seen to occur for $R_0 = 84$ mm at $\gamma = 1.8$ and for $R_0 = 112$ mm at $\gamma = 0.6$ (see Table II). For these settings, the experimental paracentric resolution gains are found to be 1.64 and 1.97 over that of the conventional HDA.

Also shown in Fig. 4 are the resolutions obtained from SIMION simulations of the full HDA plus input lens. Agreement with experiment is seen to be within 20%–30% for the cases of $R_0 = 112$ mm and 100 mm and fairly consistent between the two different simulation approaches. Such an uncertainty is typical of mechanical tolerances in the construction of HDAs.[18] However, for the case of $R_0 = 84$ mm and $\gamma > 1.5$ the discrepancy with experiment is much larger than for all other cases and therefore puzzling. While the trend in the experiment seems to be correctly depicted by the simulations, experimental results are consistently higher than simulation for $\gamma < 1.5$, but then cross over for $\gamma > 1.5$ with the simulation now seeming larger. This turnover is also seen to occur for the $R_0 = 112$ mm case around $\gamma = 0.8$. Improving the simulation grid unit (gu) density by a factor of 4 [to 0.125 mm/gu using special techniques[19] to avoid increasing RAM usage (and refine time) by a factor of 4^3 when it was already near 1 GB] for some test cases of $R_0 = 84$ mm showed only negligible differences giving us confidence that the discrepancy is not due to computational errors in the evaluation of the potentials. It should be noted that for both $R_0 = 84$ and 112 mm and for values of γ larger than the cross over points the electron trajectories increasingly hit the inner (for $R_0 = 84$ mm) or the outer (for $R_0 = 112$ mm) electrode of the HDA, thus reducing the overall transmission of the HDA. Thus, in both such cases, increasing discrepancy between simulation and experiment seems to be correlated with increased loss of transmission.

Another source of uncertainty could also arise from the length of the interaction region in the experiment, which was

TABLE II. Overall base energy resolution R_{Bs0} results for an electron source energy $E_{s0} = 200$ eV and pass energy $E_0 = 50$ eV. Comparison of lowest experimentally determined values to those from SIMION simulations and ideal field HDA theory. Values of parameters from Table I were used. A conservative estimate of 20% of R_{Bs0} was assigned to the experimental values to reflect absolute errors due to possible mechanical imperfections (see text). Resolution gain is computed with respect to the experimental resolution of the conventional fringing field HDA ($R_0 = 100$ mm, $\gamma = 1$). The HDA voltages used were computed from Eq. (1). Lens voltages used were fixed at $V_{1a} = 0$, $V_{2a} = 114.0$ V, $V_{3a} = -104.7$ V, $V_{4a} = 144.0$ V.

			Overall base energy resolution $R_{Bs0} = \Delta E_B/E_{s0}$ (%)						
			Ideal field theory			SIMION simulation			
				$\alpha_{\max}$ (Eq. (5))					
Entry radius R_0 (mm)	γ	Entry potential $V(R_0)$ (Volts)	Optimal (Eq. (7))	0°	6.5°	Beam width method	Voltage scan method	Experiment	Resolution gain
100	1.0	−150	0.284	0.500	1.79	1.35	1.40	1.36 ± 0.27	1.00
84	1.8	−110	0.458	0.822	2.11	1.22	1.60	0.83 ± 0.17	1.64
112	0.60	−170	0.184	0.314	1.60	0.47	0.50	0.69 ± 0.14	1.97

estimated to be between 1–2 mm, which is imaged by the lens onto the entry of the HDA. In all simulations a line source of $d_s = 2$ mm length along the X-direction (dispersion direction) was used giving the best agreement with experimental results. In the past, when only the HDA (without the lens) was simulated, our source always lay within the entry slit of the HDA and results depended sensitively on its extent. Large resolution gains of up to 34 were reported[4] for a point source and 4.2 for a 1 mm source, respectively. Here, it is the size of the image of the original object at the collision region as controlled by the lens magnification that lies within the entry slit. While the lens voltages were set according to best working experience with this lens, a full search for the optimal voltages giving the best resolution was not performed. Such a search can be readily carried out in simulation and could yield still further improvements in the ultimate experimental resolution gains of the paracentric HDAs.

VI. SUMMARY AND CONCLUSION

In this paper we present, for the first time, direct experimental evidence showing the energy resolution of a biased paracentric HDA to be at least a factor of 1.7–2 times better than the resolution of a conventional HDA, in support of predictions based on previous simulation work. This experimental finding is also in agreement with new simulations presented here which for the first time treat the more realistic case of a HDA with input lens under pre-retardation conditions.

The biased paracentric HDA differs from a conventional HDA in two important ways: (a) the HDA entry distance R_0 is paracentric, i.e., either larger or smaller than the mean HDA radius used in a conventional HDA and (b) the two hemispherical electrode voltages are set so that the entry potential $V(R_0)$ of the HDA is non-zero (biased), as opposed to conventional HDA usage in which this bias is typically zero. For very particular values of R_0 and $V(R_0)$, empirically found through simulations, we have shown[2] in the past that substantial improvements in energy resolution can be made, practically restoring first-order focusing conditions without the use of any additional fringing field correction electrodes, as typically done for conventional HDAs.

The above experimental validation was accomplished by a specially designed HDA with a five-element input lens for which the entry position radius R_0 (i.e., the position of the HDA entry aperture) could be readily moved and placed at any position between $R_1 = 75$ mm and $R_2 = 125$ mm, the two radii of the HDA. Thus, we experimentally determined the overall base energy resolution of this HDA for entries $R_0 = 84$, 100, 112 mm presenting results for the case of pre-retardation factor of $F = 4$ for various values of the bias $V(R_0)$ allowing for their direct inter-comparison on the same setup.

The measured improvement in energy resolution is particularly remarkable as it is conveniently attained without the use of any type of additional fringing field correction electrodes, but simply by taking advantage of the strong intrinsic lensing properties of the existing HDA fringing fields as determined and optimized by the particular paracentric entry position and bias control. Clearly, the use of fewer electrodes in the paracentric design reduces its operational complexity and lowers the overall cost of construction and HV power supplies. Improvement in energy resolution also means that paracentric HDAs of smaller size and therefore weight could replace larger conventional HDAs of equal resolution, particularly attractive to outer space instrumentation applications where both size and weight are invaluable. Finally, not having to introduce cumbersome additional correction electrodes that could partly block transmission, especially when used with a position sensitive detector, is clearly a big advantage.

ACKNOWLEDGMENTS

This work was supported on the Turkish side by the Scientific and Technological Research Council of Turkey (TUBITAK), through Grant Nos. 106T722 and 109T738. On the Greek side this research has been cofinanced by the European Union (European Social Fund—ESF) and Greek national funds through the Operational Program "Education and Lifelong Learning" of the National Strategic Reference Framework (NSRF)—Research Funding Program: THALES. Investing in knowledge society through the European Social Fund (Grant No. MIS 377289). We are also grateful to the Turkish Patent Institute for funding this work (Registration No: 2009 08700). The authors thank Dr. Omer Sise for his contribution to the initial stages of this investigation and Ahmet Deniz for his help with the technical drawings of the variable entry analyzer. Theo Zouros would also like to thank David Manura of SIS for critically reading the manuscript, as well as for his help with various SIMION 8.1 issues and Lua programming and Professor Kai Rossnagel of the University of Kiel for useful conversations. Finally, we thank Professor Genoveva Martínez López for critically reading the manuscript.

[1] T. J. M. Zouros and E. P. Benis, J. Electron Spectrosc. Relat. Phenom. **125**, 221–248 (2002); "Erratum," **142**, 175 (2005).
[2] O. Sise, T. J. M. Zouros, M. Ulu, and M. Dogan, Meas. Sci. Technol. **18**, 1853–1858 (2007).
[3] E. P. Benis and T. J. M. Zouros, Nucl. Instrum. Methods Phys. Res. A **440**, 462–465 (2000).
[4] T. J. M. Zouros, O. Sise, M. Ulu, and M. Dogan, Meas. Sci. Technol. **17**, N81–N86 (2006).
[5] O. Sise, G. Martinez, T. J. M. Zouros, M. Ulu, and M. Dogan, J. Electron Spectrosc. Relat. Phenom. **177**, 42–51 (2010); predictions of optimal paracentric conditions were found to lie at $R_0 = 85$ mm, $\gamma = 1.435$, and $R_0 = 115$ mm, $\gamma = 0.672$ for a HDA with $R_1 = 75$ mm and $R_2 = 125$ mm. Here the constructed HDA has the same electrode radii, but the entry positions could only be approximately set at $R_0 = 84$ mm and 112 mm.
[6] SIMION version 8.1.1.29, 12/29/2012, Scientific Instrument Services, Inc., Ringoes, NJ, see http://www.simion.com.
[7] E. P. Benis and T. J. M. Zouros, J. Electron Spectrosc. Relat. Phenom. **163**, 28–39 (2008). In this reference as well as in Ref. 1, two angles α are defined: α^*, the input half-angle prior to refraction by the lens/HDA interface and α the half-angle after refraction. The two are related by $\alpha = \alpha^*/\sqrt{\gamma}$ via Snell's law and/or the Helmholtz-Lagrange theorem.[8–11] Here, to avoid cumbersome notation, we just use the symbol α for what in Refs. 1 and 7 was symbolized by α^*.
[8] Volker Schmidt, *Electron Spectrometry of Atoms Using Synchrotron Radiation* (Cambridge University Press, 1997) (see Eq. (4.7a)).
[9] M. Yavor, "Optics of Charged Particle Analyzers: Chapter 6. Electrostatic energy analyzers," in *Advances in Imaging and Electron Physics* (Academic, 2009), Vol. 157, pp. 213–258.
[10] E. H. A. Granneman and M. J. Van der Wiel, "Transport, dispersion and detection of electrons, ions and neutrals," in *Handbook of Synchrotron*

Radiation, edited by E. E. Koch (North Holland, Amsterdam, 1983), Vol. 1A, Chap. 6, pp. 367–456.
[11]T. J. M. Zouros and E. P. Benis, Appl. Phys. Lett. **86**, 094105 (2005).
[12]T. J. M. Zouros, E. P. Benis, and I. Chatzakis, Nucl. Instrum. Methods Phys. Res. B **235**, 535–539 (2005).
[13]M. Dogan, M. Ulu, and O. Sise, J. Electron Spectrosc. Relat. Phenom. **161**, 58–62 (2007).
[14]M. Dogan, A. Crowe, K. Bartschat, and P. J. Marchalant, J. Phys. B **31**, 1611–1624 (1998).
[15]M. Dogan and A. Crowe, J. Phys. B **35**, 2773–2781 (2002).
[16]T. J. M. Zouros, Omer Sise, F. M. Spiegelhalder, and David J. Manura, Int. J. Mass Spectrom. **261**, 115–133 (2007).
[17]C. E. Kuyatt and J. A. Simpson, Rev. Sci. Instrum. **38**, 103–111 (1967).
[18]B. Wannberg, Nucl. Instrum. Methods Phys. Res. A **239**, 269–272 (1985).
[19]G. G. Gennarakis *et al.*, "Energy resolution of a paracentric hemispherical deflector analyzer for different entry positions and bias: Detailed Measurements and 3D Simulation," J. Electr. Spectr. Rel. Phenom. (to be published).